RSC Advances

PAPER

View Article Online
View Journal | View Issue

Cite this: *RSC Adv.*, 2018, **8**, 31581

Self-assembled pH-responsive supramolecular hydrogel for hydrophobic drug delivery

Lin Wang,[ab] Xuefeng Shi,*[a] Jian Zhang,[c] Yuejun Zhu[c] and Jinben Wang *[a]

Received 17th July 2018
Accepted 18th August 2018

DOI: 10.1039/c8ra06064a

rsc.li/rsc-advances

In this study, a novel supramolecular hydrogel system, abbreviated as AGC_{16}/NTS, prepared by molecular self-assembly of cationic gemini surfactant 1,3-bis(*N*,*N*-dimethyl-*N*-cetylammonium)-2-propylacrylatedibromide (AGC_{16}) and anionic aromatic compound trisodium 1,3,6-naphthalenetrisulfonate (NTS), was used to encapsulate hydrophobic model drug curcumin (Cur), constructing a pH-responsive drug delivery system. Cur was effectively encapsulated into the hydrophobic domains of AGC_{16}/NTS through hydrophobic interaction, which was confirmed by ^{1}H NMR measurement. The effects of Cur on the mechanical strength, phase transition behaviour and morphology of AGC_{16}/NTS were characterized by rheology and cryogenic scanning electron microscopy (cryo-SEM) methods. The pH-responsive release of Cur from AGC_{16}/NTS was obtained and the release amount of Cur ascended with pH value decreasing from 7.4 to 3.0. The hydrodynamic sizes of the released Cur-aggregates determined by dynamic light scattering (DLS) were used to analyse the release process of Cur at different pH. The cell viability assay and cell imaging experiment demonstrated that Cur-loaded hydrogel has much higher cytotoxicity and better cell uptake compared to free Cur. Overall, the AGC_{16}/NTS hydrogel is a prospective material for use in encapsulation and controlled-release of hydrophobic drug molecules.

1 Introduction

Many supramolecular materials, such as nanoparticles, polymeric micelles, lipids, hydrogels *etc.*, have been used as carriers of target drugs to greatly enhance their water solubility and stability and prolong their circulation in blood compartments.[1] Among these materials, hydrogels are able to retain an inherently biocompatible water environment, which resembles natural living tissues, and have the potential to be drug delivery systems.[2–4] Different from polymeric hydrogels, supramolecular hydrogels based on low-molecular-weight gelators are easily constructed by noncovalent interactions, such as H-bonding, π-stacking and van der Waals forces, under mild conditions in absence of initiators and crosslinking agents.[5–8] In the meantime, supramolecular hydrogels can quickly respond to external stimuli due to the dynamic and reversible nature of the noncovalent interactions compared to the covalent systems, resulting in a stimuli-responsive cargo delivery carrier.[9–11]

As far as we know, widely used anticancer drugs such as paclitaxel, camptothecin and platinum compounds have limited water solubility which restrict their applications in cancer chemotherapy. The hydrophilic microstructures of supramolecular hydrogels typically make it difficult to load hydrophobic drugs.[12,13] It is also known that tumour tissues present an acidic environment relative to normal tissue.[14] The difference in pH between tumour tissues and normal tissues is advantageous for the controlled release of drugs at the specific targeting tumour site. As far as we know, there is relatively less literature on supramolecular hydrogel which could simultaneously satisfy the above-mentioned aspects. Thus, designing and constructing supramolecular hydrogel system used to encapsulate and release hydrophobic anticancer drug in response to pH is not only fundamentally important for mechanisms behind drug delivery, but also practically valuable for the development of efficient controlled release materials.

Gemini surfactants have attracted considerable attention due to lower critical micelle concentration (cmc), special aggregation behaviour and significant application in drug delivery.[15] As the cmc value of gemini surfactants is very low, less amounts of molecules of gemini surfactants than corresponding monomeric surfactants are used to construct hydrogels, which is an advantage of gemini surfactant in hydrogel preparation. Covalent connection between charged head groups promotes the formation of aggregates in water. These aggregations with hydrophobic domains could improve the solubility of hydrophobic drug through hydrophobic interaction.[16–18]

Based on these above considerations, we prepared a supramolecular hydrogel by mixing of gemini surfactant 1,3-bis (*N*,*N*-dimethyl-*N*-cetylammonium)-2-propylacrylate dibromide

[a]*CAS Key Laboratory of Colloid, Interface and Chemical Thermodynamics, Institute of Chemistry, Chinese Academy of Sciences, Beijing 100190, P. R. China. E-mail: jbwang@iccas.ac.cn; xfshi@iccas.ac.cn; Fax: +86-10-62523395; Tel: +86-10-62523395; +86-10-62652659*

[b]*University of Chinese Academy of Sciences, Beijing 100049, P. R. China*

[c]*State Key Laboratory of Offshore Oil Exploitation, CNOOC Research Institute Co. Ltd., Beijing 100028, P. R. China*

(AGC_{16}) (chemical structure shown in Fig. 1a) and anionic trisodium 1,3,6-naphthalenetrisulfonate (NTS) (Fig. 1b). The pH-responsive supramolecular hydrogel could be formed within a few minutes in aqueous medium. The certain length hydrocarbon chains of AGC_{16} are indispensably needed to easily construct the hydrophobic domains during gel formation, enhancing the encapsulation ability of hydrophobic drug through hydrophobic interaction. Besides, at lower pH value, the protonation of the sulfonates ($-SO_3^-$) of NTS within AGC_{16}/NTS leads to decrease the electrostatic interaction between the $-SO_3^-$ of NTS and $-NH_4^+$ of AGC_{16}, accelerating the dissociation of hydrogels and drug fast release from AGC_{16}/NTS. Curcumin (Cur) (Fig. 1c) possesses antioxidant, anti-inflammatory, anti-tumor, anti-HIV, and antimicrobial properties, but its application in cancer therapy is limited because of its low aqueous solubility (~11 ng mL^{-1}).[19–21] Herein, Cur was chosen as a model drug to study the effect of Cur on the self-assembly of gelators and the drug release behavior of AGC_{16}/NTS at pH ranging from 3 to 7.4. The cell viability assay and cell imaging experiment were also studied. Schematic representation of pH-responsive release Cur from AGC_{16}/NTS hydrogel and the uptake of Cur by cancer cells is shown in Fig. 2. These results indicate that AGC_{16}/NTS hydrogel has a great potential as a pH-responsive hydrophobic drug delivery carrier.

2 Experimental section

2.1 Materials

Trisodium 1,3,6-naphthalenetrisulfonate (NTS) was obtained from Tianjin Alfa Aesar Chemical Reagent Company, China. Curcumin (Cur) was supplied from Shanghai Energy Chemical Reagents Company, China. All the reagents were of AR grade and used without further purification. AGC_{16} was synthesized in our laboratory using a previously reported method.[22] All solutions were prepared with Milli-Q gradient ultrapure water.

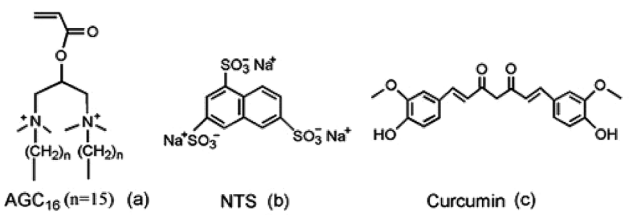

Fig. 1 The chemical structures of AGC_{16} (a), NTS (b), and Cur (c).

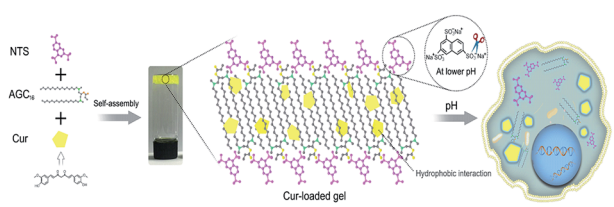

Fig. 2 Schematic representation of pH-responsive release of Cur from AGC_{16}/NTS hydrogel and the uptake of Cur by cancer cells.

2.2 Preparation of supramolecular hydrogel AGC_{16}/NTS

Supramolecular hydrogel AGC_{16}/NTS was prepared by directly mixing the AGC_{16} solution and NTS solution. Firstly, AGC_{16} aqueous solution (0.037 M) was prepared and then kept at 60 °C to obtain a clear solution. Then, 50 μL of NTS aqueous solution (0.23 M) was added into 1.67 mL of AGC_{16} solution under vigorous stirring at 60 °C. Finally, the mixture was cooled down to room temperature, followed by degassing under vacuum for 1 min, the supramolecular hydrogel AGC_{16}/NTS was formed.

2.3 Drug encapsulation and release

Preparation of Cur-loaded hydrogel was described as follows. Firstly, Cur (100 mg, 0.27 mmol) was dissolved in 1 mL of THF. Then, 10 μL of Cur solution (271.4 mM), 1.67 mL of AGC_{16} solution (37.1 mM) and 50 μL of NTS solution (230.4 mM) were mixed thoroughly at 65 °C by vigorous stirring to obtain homogeneous dispersion of the drugs within AGC_{16}/NTS, and then the mixture was placed in a desiccator under vacuum to evaporate the organic solvents. After the mixed solution was slowly cooled down to room temperature, the Cur-loaded hydrogel was obtained. The loading amount of Cur within 1.0 g hydrogel is 0.6 mg.

The release curve of Cur from AGC_{16}/NTS was measured at physiological temperature condition (37 °C) as follows. 500 mg of Cur-loaded hydrogel (0.3 mg Cur) was put in a bottle containing 100 mL of a phosphate buffer solution (10 mM) of pH 3, 5.5 and 7.4, and then the bottle was placed in an incubator shaker at 37 °C. At regular intervals, 2.0 mL of the supernatant solution was withdrawn, and followed by the addition of an equal amount of buffer solution to keep the constant volume of the medium. The cumulative release amount of Cur from the gel was determined by monitoring the variation of the concentration of Cur. The concentration of Cur was monitored by UV-vis spectrophotometer at the wavelength of 422 nm.

2.4 *In vitro* cell studies

2.4.1 Cell culture. HeLa cells and HepG-2 cells were cultured in DMEM supplemented with 10% fetal bovine serum at 37 °C in a humidified incubator containing 5% CO_2.

2.4.2 *In vitro* cytotoxicity assay. The cells were seeded in 96-well plates at a density of 5×10^3 cells per well. After 12 hours incubation, the medium was replaced by various concentrations of three different compounds (Cur, AGC_{16}/NTS xerogel, and Cur-loaded AGC_{16}/NTS xerogel) in culture medium and the cells were further cultured for 24 h. Then the medium was discarded and 0.5 mg mL^{-1} MTT in culture medium was added to each well. After incubation for 4 hours, DMSO was added to each well. The absorbance values of each well at 570 nm were measured by a microplate reader. Cell viability rate (VR) is defined as the percentage of the absorbance values of the wells incubated with drug (A) over that of the control wells incubated with culture medium only (A_0). The equation is as follow:

$$\mathrm{VR} = \frac{A}{A_0} \times 100\%$$

2.4.3 Cell imaging. HeLa cells and HepG-2 cells were seeded in 20 mm glass bottom cell culture and dished at a density of 1×10^5 cells per dish, and further cultured for 12 h. Then free Cur in medium (0.2 μg mL^{-1}), AGC_{16}/NTS in medium (10 μg mL^{-1}) and Cur-loaded AGC_{16}/NTS in medium (10 μg mL^{-1}, equivalent Cur concentration) were added to the adherent cells. After incubation for 24 h, cells were washed twice with 1× PBS buffer and imaged immediately by confocal laser scanning microscopy (CLSM) (Olympus FV 1200-BX61, Japan). The excitation wavelength of AGC_{16}/NTS, Cur-loaded AGC_{16}/NTS, and Cur is 405 nm.

2.5 Characterization

2.5.1 Rheology. Rheological measurements of AGC_{16}/NTS and Cur-loaded AGC_{16}/NTS were performed under oscillatory condition on a AR2000 Ex rheometer (TA instruments Ltd. USA). Samples were placed between parallel plates (diameter, 20 mm) and a gap of 1.0 mm. The temperature was controlled using Peltier system with the bottom plate connected to a water bath. All the oscillatory measurements were performed within the linear viscoelastic range. The instrumental setups for the rheology tests are the following:

A frequency-sweep measurement from 0.1 to 100 rad s^{-1} was conducted at room temperature using a constant strain of 0.1%. Strain-sweep measurement from 0.1 to 100% was performed at room temperature using a fixed angular frequency of 10 rad s^{-1}.

2.5.2 Cryogenic scanning electron microscopy and transmission electron microscopy. AGC_{16}/NTS and Cur-loaded AGC_{16}/NTS images were taken on a S-4300 cryogenic scanning electron microscopy (cryo-SEM) (Hitachi Ltd., Japan) at an acceleration voltage of 3 kV and a beam current of 10 μA. The AGC_{16}/NTS and Cur-loaded hydrogel were "sandwiched" between two gold planchettes, respectively, then plunged into a liquid nitrogen slush, and then transferred under vacuum into cryo-preparation chamber (LEICA EM ACE600). The samples were sublimed in this station at −100 °C for 10 min. The frozen sample surfaces were then sputter coated with Pt in an argon environment (15 mA for 200 s) to make them conductive. After that, samples were transferred from the workstation to the cryostage in the microscope and held at −137 °C. The morphology of Cur-aggregates was observed using JEM-1011 transmission electron microscope (TEM) (JEOL Ltd., Japan) at a working voltage of 100 kV. The TEM sample was prepared by the negative-staining method. Cur-aggregates solution was applied onto the carbon-coated copper grid (400 mesh) for 5 min, then using filter paper to wick off excess fluid. Next, the copper grid was laid onto one drop of uranyl acetate solution (0.5%) as the staining agent. The excess liquid was removed with filter paper and the sample was dried at room temperature.

2.5.3 ^{1}H nuclear magnetic resonance spectra. ^{1}H Nuclear Magnetic Resonance (^{1}H NMR) spectra were performed on a 500 MHz Bruker AVANCE III spectrometer (Bruker Ltd., Switzerland). The ^{1}H NMR spectra of AGC_{16} with $CDCl_3$ as solvent, AGC_{16}/NTS and Cur-loaded AGC_{16}/NTS hydrogel with D_2O as solvent were recorded at 25 °C.

2.5.4 Dynamic laser scattering and zeta potential measurements. The hydrodynamic sizes of the Cur-aggregations were determined by dynamic laser scattering (DLS) with a Zetasizer Nano ZS (Malvern Instruments Ltd., UK) at $\lambda = 532$ nm with a fixed detector angle of 90°. Each size value was derived from the average of three measurements. The zeta potential of $-SO_3^-$ of NTS at different pH was determined using a Zetasizer Nano ZS (Malvern Instruments Ltd., UK).

3 Results and discussion

3.1 Effect of Cur on the self-assembly of gelators

3.1.1 Rheology. Dynamic Frequency Sweep (DFS) and Dynamic Strain Sweep (DSS) measurements were used to explore the difference of rheological strength between AGC_{16}/NTS and Cur-loaded AGC_{16}/NTS.[23] Fig. 3a shows the frequency dependence of elastic modulus (G') and viscous modulus (G'') of AGC_{16}/NTS and Cur-loaded AGC_{16}/NTS. It is clearly indicated that both AGC_{16}/NTS and Cur-loaded AGC_{16}/NTS are in gel state ($G' > G''$). Moreover, the encapsulation of Cur has an effect on the mechanical strength of AGC_{16}/NTS. G' of Cur-loaded AGC_{16}/NTS is an approximately 8-fold lower than that of AGC_{16}/NTS at the measured angular frequency range, which could be explained by the fact that the larger steric hindrance of the Cur interferes the ordered packing of gelators and thus resulting in a decrease in hydrogel mechanical strength of the hydrogel.[24]

Fig. 3b shows the DSS data for AGC_{16}/NTS and Cur-loaded AGC_{16}/NTS. AGC_{16}/NTS possesses a critical strain value ($G' = G''$) of 50%, above which the elastic regime of gel ($G' > G''$) disappeared and a viscous regime occurred ($G'' > G'$) owing to the disruption of the gel network when the yield strain of the network is exceeded.[25] As for Cur-loaded AGC_{16}/NTS, the critical strain value is only 30%, demonstrating a lower mechanical strength of Cur-loaded AGC_{16}/NTS than that of AGC_{16}/NTS.

3.1.2 Morphology. Cryo-SEM measurement was used to observe the hydrogel morphology and the variation of the aggregates conformation, facilitating further understanding the effect of Cur on the self-assembly of gelators.[26] Fig. 4a shows that the morphology of AGC_{16}/NTS exhibits a network structure consisting of micrometer-sized porous cavities which are composed of intertwined sheets filled with a large amount of small assemblies. A closer examination in Fig. 4b indicates that the assemblies are formed by tightly packed or aggregated

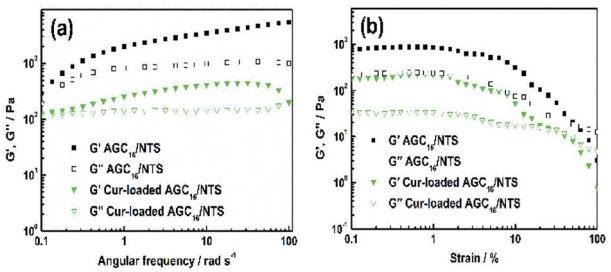

Fig. 3 (a) Dynamic frequency-sweep (DFS) rheological data and (b) dynamic strain-sweep (DSS) rheological data of AGC_{16}/NTS and Cur-loaded gel at room temperature.

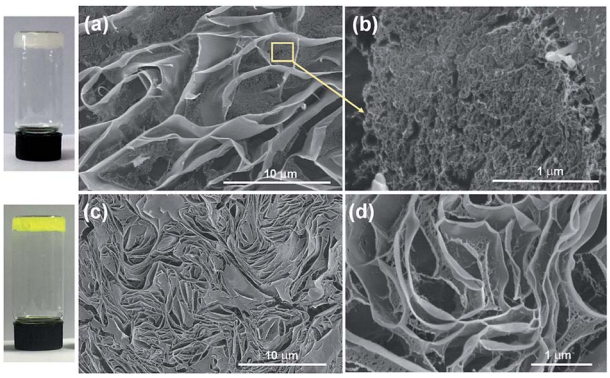

Fig. 4 Cryo-SEM images of (a and b) AGC_{16}/NTS and (c and d) Cur-loaded AGC_{16}/NTS hydrogel.

individual fiber. Fig. 4c and d show the cryo-SEM images of Cur-loaded AGC_{16}/NTS hydrogel which exhibit no grain structure or grain boundary indicating that Cur had been encapsulated into AGC_{16}/NTS rather than undergoing physical mixing. As shown in Fig. 4c, the morphology of Cur-loaded AGC_{16}/NTS contains a similar network structure as AGC_{16}/NTS, which is also composed of interconnected cavities with smaller size than that of AGC_{16}/NTS. Different from AGC_{16}/NTS, it is found that no dense fiber aggregates exist within the porous structures (Fig. 4d), which could be the reason for a lower mechanical strength compared with that of AGC_{16}/NTS, similar to the effect of inorganic fillers on the mechanical strength of rubber.

3.1.3 Phase transition behavior. Variable-temperature rheology was carried out to explore the phase transition temperatures of AGC_{16}/NTS and Cur-loaded AGC_{16}/NTS.[27] As shown in Fig. 5a, above 57 °C, G'' is larger than G', indicating that the mixture of AGC_{16} and NTS is in sol state, thus the gel–sol transition temperature of AGC_{16}/NTS is ~57 °C. As for Cur-loaded AGC_{16}/NTS (Fig. 5b), the gel–sol transition temperature ($G'' > G'$) is 49 °C. The decrease of gel–sol transition temperature for Cur-loaded AGC_{16}/NTS is due to that the larger steric hindrance of the Cur interferes the ordered packing of gelators and thus Cur-loaded AGC_{16}/NTS with lower mechanical strength is easier to transform to sol at a lower temperature than AGC_{16}/NTS. The change of gelators packing also leads to disappeared fiber aggregates filled in porous cavities of Cur-loaded AGC_{16}/NTS.

3.1.4 Encapsulation of Cur into hydrophobic domains. The presence of hydrophobic interaction between drug curcumin and gelator AGC_{16} was characterized by ^{1}H NMR spectra.[28] Fig. 6

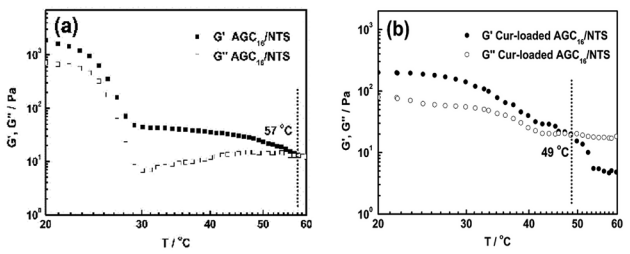

Fig. 5 Rheological measurement data of AGC_{16}/NTS (a) and Cur-loaded AGC_{16}/NTS (b) from 20 °C to 60 °C.

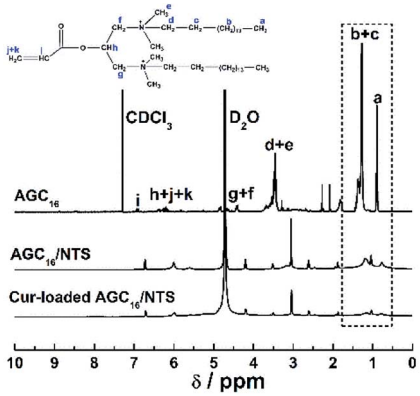

Fig. 6 ^{1}H NMR spectra of AGC_{16}/NTS gel and Cur-loaded AGC_{16}/NTS gel.

shows the ^{1}H NMR spectroscopy of AGC_{16} in $CDCl_3$, AGC_{16}/NTS gel and Cur-loaded gel in D_2O at 25 °C. AGC_{16} in $CDCl_3$ shows sharp alkyl proton (H_{a-c}) peaks at 0.88 ppm and 1.27 ppm, while these peaks from AGC_{16}/NTS hydrogel become broad and weak. This indicates the restricted freedom of thermal motion of alkyl chains that are arranged into hydrophobic domain through hydrophobic interaction in hydrogel state.[29] When Cur was encapsulated into AGC_{16}/NTS, the alkyl proton (H_{a-c}) signals from alkyl chains of Cur-loaded AGC_{16}/NTS are further weak indicating that a new hydrophobic aggregate formed by self-assembly of gelators and Cur molecules through hydrophobic interaction. The new aggregate with high packing density further minimizes interaction with D_2O, resulting in obviously suppressed alkyl proton (H_{a-c}) signals. Thus, these results demonstrated that Cur was encapsulated within hydrophobic domains formed by the certain length hydrocarbon chains of AGC_{16} through hydrophobic interaction.[30]

3.2 pH-responsive release of Cur

3.2.1 Release behavior of Cur. The release behaviour of Cur was studied by the cumulative release amount in PBS buffer solution with pH 3, 5.5 and 7.4 at 37 °C. As shown in Fig. 7a, a considerable decrease of cumulative release of Cur occurred with increasing pH value from 3 to 7.4. For initial 7 h at pH 7.4, AGC_{16}/NTS remains more stable than that at pH 5.5 and 3 and no Cur was released into the external medium. After 15 h, the release of Cur reaches up to ~35%, while the release of Cur at pH 5.5 and 3 are up to 70% and 97%, respectively. The above release processes of Cur were also distinctly observed in Fig. 7b. These phenomena could be attributed to the fact that the sulfonates ($-SO_3^-$) of NTS are protonated ($-SO_3H$) at the lower pH (tumor tissues) and the electrostatic interaction between $-SO_3^-$ and cationic gelator AGC_{16} is weakened, resulting in the accelerated dissociation of hydrogels and then drug release.[31] To verify the above conclusion, we measured the zeta potential of $-SO_3^-$ of NTS at different pH, as shown in Fig. 7c. At pH 3, the zeta potential of $-SO_3^-$ presents lower negative charge (−5.07 mV) than that at pH 5.5 (−18.4 mV) and pH 7.4 (−28.5 mV). The lower negative charge demonstrates the stronger protonation of

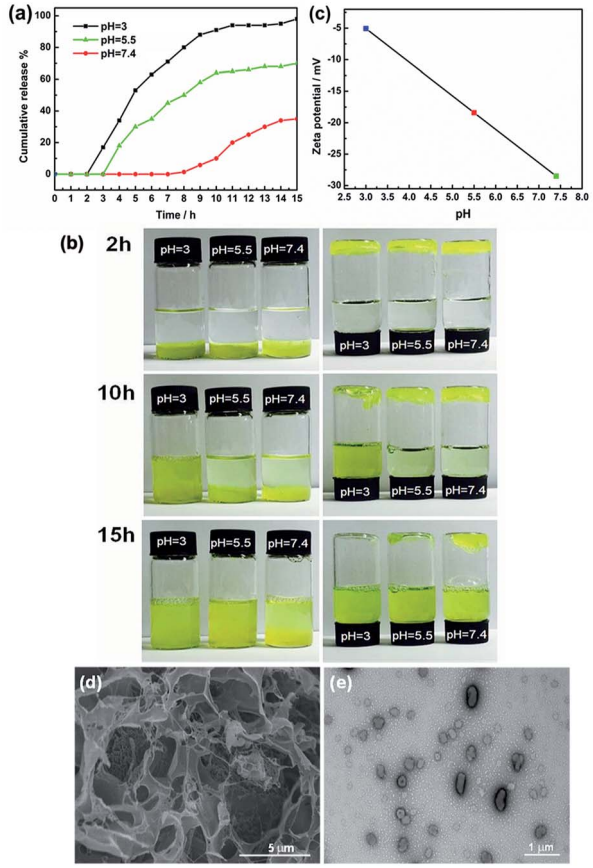

Fig. 7 (a) Release curves of Cur from AGC_{16}/NTS gel at different pH. (b) Images of Cur release from AGC_{16}/NTS gel at different pH. (c) Zeta potential of SO_3^- of NTS as a function of pH. (d) Cryo-SEM image of AGC_{16}/NTS after drug release under pH 5.5 at 5 h. (e) TEM image of Cur-aggregates under pH 5.5 at 15 h.

$-SO_3^-$ which has weaker electrostatic interaction with AGC_{16}, accelerating the dissociation of hydrogels at lower pH.[32]

The morphology changes of AGC_{16}/NTS after Cur release were observed by cryo-SEM and TEM. At acidic environment, such as pH 5.5 at 5 h, cryo-SEM image (Fig. 7d) shows that the remaining AGC_{16}/NTS presents an irregular morphology, which is different from the order network structure of Cur-loaded AGC_{16}/NTS, indicating that AGC_{16}/NTS was dissociated. With the time increasing to 15 h, AGC_{16}/NTS is in almost complete dissociation state and released Cur exists in the form of Cur/AGC_{16}/NTS aggregations (Cur-aggregations) in external medium. TEM image (Fig. 7e) exhibits that the Cur-aggregations has a similar spherical morphology with a size of around 500–700 nm, which is consistent with the DLS results.

3.2.2 The release mechanism of Cur. Due to the insolubility of Cur in aqueous medium, released Cur exists in the form of Cur/AGC_{16}/NTS aggregation (Cur-aggregations) in external medium. DLS measurement was utilized to investigate the release mechanism of Cur by determining the hydrodynamic size changes of Cur-aggregations. As shown in Fig. 8a, within the initial 2 h at pH 3 when no Cur was released from Cur-loaded hydrogel, the determined size values were attributed to gelators (AGC_{16} and NTS) aggregates instead of Cur-aggregations and there are no significant size changes during the dissociation process of Cur-loaded hydrogel. The reason of this phenomenon could be a weaker interaction between released gelators and Cur than that between remaining gelators within hydrogel and Cur. With the time increasing from 2 h to 10 h, the sizes of the released Cur-aggregations increase from 400 nm to 800 nm, which could be attributed to increasing amount of Cur carried away by gelators aggregates. After 10 h, the size changes of Cur-aggregations is not obvious, corresponding to the release equilibrium of Cur. In Fig. 8b and c, as for pH 5.5, the size of Cur-aggregations gradually increases from 310 nm to 625 nm during the releasing period of 2–15 h, while there are no significant size changes of Cur-aggregations at pH 7.4. The results show that the release of Cur ascends with pH decreasing from 7.4 to 3.0, which is consistent with the release curves in Fig. 7a.

3.3 Cytotoxicity assay and cell imaging

The cytotoxicity of Cur-loaded AGC_{16}/NTS, AGC_{16}/NTS and free Cur against HeLa and HepG-2 cells were investigated by MTT assay. As shown in Fig. 9a, free Cur and AGC_{16}/NTS exhibits a minimal cytotoxicity against HeLa cells. However, Cur-loaded AGC_{16}/NTS shows a significantly enhanced cytotoxicity compared to AGC_{16}/NTS and free Cur at an equal concentration. Especially, in the concentration range from 8 μg mL^{-1} to 32 μg mL^{-1}, the cytotoxicity of Cur-loaded AGC_{16}/NTS obviously increases whereas that of AGC_{16}/NTS and free Cur remain almost unchanged. And, as for HepG-2 cells, Cur-loaded AGC_{16}/NTS also exhibits significantly higher cytotoxicity than that of AGC_{16}/NTS and free Cur (Fig. 9b).

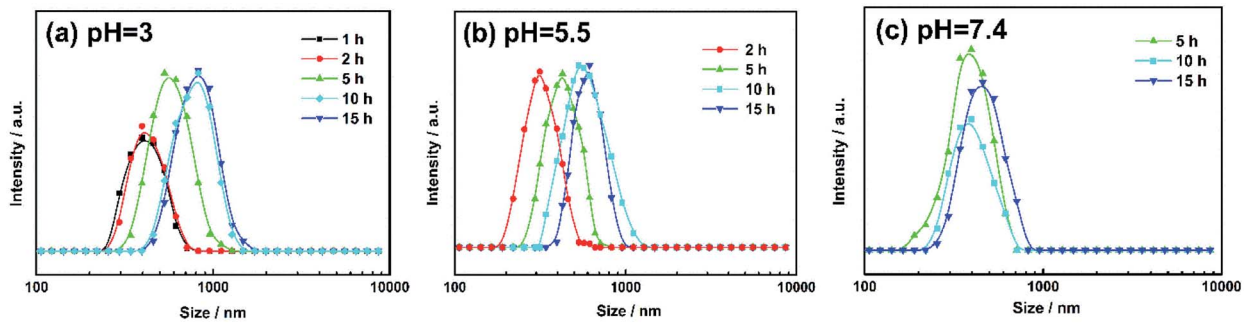

Fig. 8 Size changes of Cur-aggregations released from Cur-loaded hydrogels at pH 3 (a), 5.5 (b) and 7.4 (c).

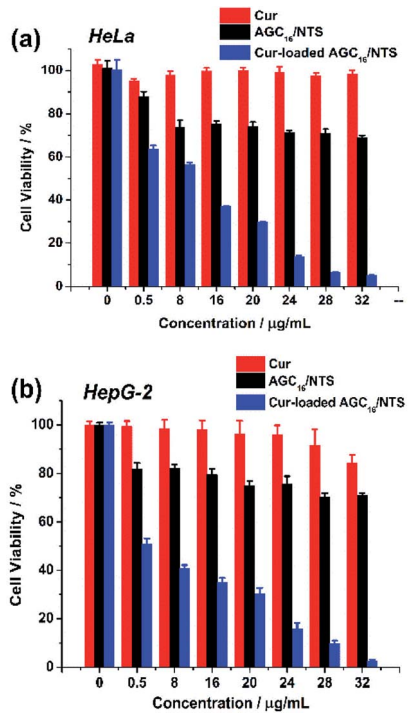

Fig. 9 Cell viability of (a) HeLa cells and (b) HepG-2 cells after incubation with various concentration of Cur-loaded AGC_{16}/NTS, AGC_{16}/NTS and free Cur ([Cur]/[AGC_{16}/NTS] = 1/50).

This result is attributed to that the formation of hydrophobic domains constructed by hydrocarbon chains of AGC_{16} improve the solubility of Cur by hydrophobic interaction, resulting in high cytotoxicity effect of Cur-loaded AGC_{16}/NTS than free Cur.

The cell imaging of Cur-loaded AGC_{16}/NTS, AGC_{16}/NTS and free Cur in HeLa and HepG-2 cells were studied using CLSM and the excitation wavelength was 405 nm. Cur itself has fluorescence, so it could investigate the cellular uptake of Cur by fluorescence images.

As seen from Fig. 10, no fluorescence signal of free Cur and AGC_{16}/NTS was observed, however, the Cur-loaded AGC_{16}/NTS exhibits fluorescence signal inside cells indicating that Cur-loaded AGC_{16}/NTS entered the cells successfully. This phenomenon is attributed to that the solubility of Cur is improved through encapsulation by hydrogel, thus, the Cur-loaded AGC_{16}/NTS is much easier than hydrophobic Cur in entering the cells to exert its cytotoxic effect and cause fatal damage.

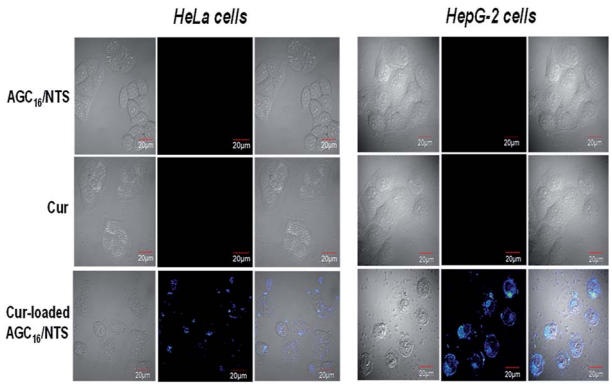

Fig. 10 CLSM images of HeLa cells and HepG-2 cells treated with AGC_{16}/NTS at 10 μg mL^{-1}, free Cur at 0.2 μg mL^{-1} and Cur-loaded AGC_{16}/NTS at 10 μg mL^{-1}.

4 Conclusion

In summary, a pH-responsive supramolecular hydrogel was successfully prepared by self-assembly of gemini surfactant AGC_{16} and anionic aromatic compound NTS, which could load the hydrophobic drug Cur to exhibit its high anticancer activity. DSS and DFS analysis results revealed that Cur-loaded AGC_{16}/NTS has a lower mechanical strength than AGC_{16}/NTS. Cryo-SEM observation and rheology measurements demonstrated that the fiber aggregates play a significant role in mechanical strength and phase transition behavior. The release experiment indicated that the AGC_{16}/NTS exhibited a pH-responsive release behaviour and the release of Cur ascended with pH decreasing from 7.4 to 3.0. MTT assay revealed that Cur-loaded hydrogel has much higher cytotoxicity against HeLa cells and HepG-2 cells than free Cur. And confocal microscopy observation showed that Cur entered into the HeLa and HepG-2 cells treated with Cur-loaded AGC_{16}/NTS. The above results show that the pH-responsive AGC_{16}/NTS hydrogel is promising as a smart carrier for loading and delivering hydrophobic anticancer drugs.

Conflicts of interest

There are no conflicts to declare.

Acknowledgements

This work was funded by the Important National Science and Technology Specific Project of China (2016ZX05025-003-009). This work also received financial support from the Strategic Priority Research Program of CAS (XDB22030102) and the National Research Project of China (2017ZX05013-003).

References

1 J. Gao, C. Xie, M. Zhang, X. Wei, Z. Yan, Y. Ren, M. Ying and W. Lu, *Nanoscale*, 2016, **8**, 7209–7216.
2 V. Kozlovskaya, J. Chen, C. Tedjo, X. Liang, J. Campos-Gomez, J. Oh, M. Saeed, C. T. Lungu and E. Kharlampieva, *J. Mater. Chem. B*, 2014, **2**, 2494–2507.
3 L. Yin, S. Xu, Z. Feng, H. Deng, J. Zhang, H. Gao, L. Deng, H. Tang and A. Dong, *Biomater. Sci.*, 2017, **5**, 698–706.
4 J. Kim, J. Hwang, Y. Seo, Y. Jo, J. Son, T. Paik and J. Choi, *J. Ind. Eng. Chem.*, 2016, **42**, 121–125.
5 S. Gupta, M. Singh, M. A. Reddy, P. S. Yavvari, A. Srivastava and A. Bajaj, *RSC Adv.*, 2016, **6**, 19751–19757.
6 C. Wang, Y. Duan, N. S. Zacharia and B. D. Vogt, *Soft Matter*, 2017, **13**, 1161–1170.
7 A. Nakagawa, F. Steiniger, W. Richter, A. Koschella, T. Heinze and H. Kamitakahara, *Langmuir*, 2012, **28**, 12609–12618.

8 K. Lalitha, V. Sridharan, C. U. Maheswari, P. K. Vemula and S. Nagarajan, *Chem. Commun.*, 2017, **53**, 1538–1541.
9 A. K. Bandela, V. K. Hinge, D. S. Yarramala and C. P. Rao, *ACS Appl. Mater. Interfaces*, 2015, **7**, 11555–11566.
10 Z. Liu and P. Yao, *Polym. Chem.*, 2014, **5**, 1072–1081.
11 W. Ha, X.-B. Zhao, K. Jiang, Y. Kang, J. Chen, B.-J. Li and Y.-P. Shi, *Chem. Commun.*, 2016, **52**, 14384–14387.
12 W. Ha, J. Yu, X.-Y. Song, Z.-J. Zhang, Y.-Q. Liu and Y.-P. Shi, *J. Mater. Chem. B*, 2013, **1**, 5532–5538.
13 F. Li, J. He, M. Zhang and P. Ni, *Polym. Chem.*, 2015, **6**, 5009–5014.
14 J. H. Jeong, J. J. Schmidt, C. Cha and H. Kong, *Soft Matter*, 2010, **6**, 3930–3938.
15 D. Kumar, N. Azum, M. A. Rub and A. M. Asiri, *J. Mol. Liq.*, 2018, **262**, 86–96.
16 X. Pei, J. Zhao, Y. Ye, Y. You and X. Wei, *Soft Matter*, 2011, **7**, 2953–2960.
17 K. Sakai, K. Ohno, K. Nomura, T. Endo, K. Sakamoto, H. Sakai and M. Abe, *Langmuir*, 2014, **30**, 7654–7659.
18 M. A. Rub, A. M. Asiri, A. Z. Naqvi, M. M. Rahman, S. B. Khan and D. Kabir ud, *J. Mol. Liq.*, 2013, **177**, 19–25.
19 M. Liu, Y. Chang, J. Yang, Y. You, R. He, T. Chen and C. Zhou, *J. Mater. Chem. B*, 2016, **4**, 2253–2263.
20 N. Madusanka, K. M. N. de Silva and G. Amaratunga, *Carbohydr. Polym.*, 2015, **134**, 695–699.
21 D. Bajani, J. Dey, Y. Rajesh, S. Bandyopadhyay and M. Mandal, *J. Colloid Interface Sci.*, 2017, **507**, 1–10.
22 Y. Wu, H. Yan, X. Shi and J. Wang, *Soft Matter*, 2017, **13**, 1881–1887.
23 J. Xu, D. Yang, W. Li, Y. Gao, H. Chen and H. Li, *Polymer*, 2011, **52**, 4268–4276.
24 R. Liang, Z. Luo, G. Pu, W. Wu, S. Shi, J. Yu, Z. Zhang, H. Chen and X. Li, *RSC Adv.*, 2016, **6**, 76093–76098.
25 H. Thérien-Aubin, Y. Wang, K. Nothdurft, E. Prince, S. Cho and E. Kumacheva, *Biomacromolecules*, 2016, **17**, 3244–3251.
26 H. Ge, C.-L. Zhao, S. Porzio, L. Zhuo, H. T. Davis and L. E. Scriven, *Macromolecules*, 2006, **39**, 5531–5539.
27 K. Nagahama, A. Takahashi and Y. Ohya, *React. Funct. Polym.*, 2013, **73**, 979–985.
28 G.-B. Jiang, D. Quan, K. Liao and H. Wang, *Mol. Pharm.*, 2006, **3**, 152–160.
29 J. Zhao, H. Wang, J. Liu, L. Deng, J. Liu, A. Dong and J. Zhang, *Biomacromolecules*, 2013, **14**, 3973–3984.
30 N. Bailly, M. Thomas and B. Klumperman, *Biomacromolecules*, 2012, **13**, 4109–4117.
31 B. V. Shankar and A. Patnaik, *J. Phys. Chem. B*, 2007, **111**, 9294–9300.
32 Y. Li, J. Lin, X. Yang, Y. Li, S. Wu, Y. Huang, S. Ye, L. Xie, L. Dai and Z. Hou, *ACS Appl. Mater. Interfaces*, 2015, **7**, 17573–17581.